Development of the Line-Focus-Beam Ultrasonic Material Characterization System

Jun-ichi Kushibiki, *Member, IEEE*, Yuu Ono, *Member, IEEE*,
Yuji Ohashi, and Mototaka Arakawa, *Member, IEEE*

***Abstract*—A line-focus-beam ultrasonic material characterization (LFB-UMC) system has been developed to evaluate large diameter crystals and wafers currently used in electronic devices. The system enables highly accurate detection of slight changes in the physical and chemical properties in and among specimens. Material characterization proceeds by measuring the propagation characteristics, viz., phase velocity and attenuation, of Rayleigh-type leaky surface acoustic waves (LSAWs) excited on the water-loaded specimen surface. The measurement accuracy depends mainly upon the translation accuracy of the mechanical stages used in the system and the stability of the temperature environment. New precision mechanical translation stages have been developed, and the mechanical system, including the ultrasonic device and the specimen, has been installed in a temperature-controlled chamber to reduce thermal convection and conduction at the specimen. A method for precisely measuring temperature and longitudinal velocity in the water couplant has been developed, and a measurement procedure for precisely measuring the LSAW velocities has been completed, achieving greater relative accuracy to better than ±0.002% at any single chosen point and ±0.004% for two-dimensional measurements over a scanning area of a 200-mm diameter silicon single-crystal substrate. The system was developed to address various problems arising in science and industry associated with the development of materials and device fabrication processes.**

I. Introduction

Evaluation techniques of material properties and device fabrication processes associated with research and development of new device materials and devices in electronics science and industry are of extreme importance, as the ultimate performance of these devices depends primarily upon the quality of materials and secondarily upon the technology of the device fabrication processes. At present, it is of the greatest importance to produce higher quality, larger diameter substrates of semiconductor single crystals such as silicon (Si) and gallium arsenide (GaAs) and of ferroelectric single crystals such as lithium niobate ($LiNbO_3$) and lithium tantalate ($LiTaO_3$), with homogeneity of their chemical and physical properties in and among crystals and substrates. It is also essential to develop and establish fabrication processes for higher quality layered media, such as epitaxial layers, amorphous layers, passivation layers, and ion-implanted layers, which are associated with device configurations. Furthermore, thin film properties, including adhesion and residual stresses at the interfaces between film layers and substrates and surface damage introduced to the surfaces of the substrates during the fabrication processes such as slicing and polishing, greatly affect performance of the devices such as super large scale integrated and high speed electronic devices, ultra high frequency (UHF) and super high frequency (SHF) surface acoustic wave (SAW) devices, and surface waveguide-type optical devices that utilize the material properties within a few microns beneath the surface. To contribute to the resolution of these problems, it is of fundamental importance to accurately analyze and evaluate the properties of materials and the device fabrication processes. Thus, it is necessary to develop new analytic and evaluation techniques enabling highly accurate detection of slight changes in the physical and chemical properties on a microscopic scale over an entire surface of bulk materials and thin film materials on large diameter substrates. It is also necessary to improve the conventional methods using X-rays, electron beams, infrared radiation, and visible light or to utilize such new methods as the scanning-tunneling microscope (STM) and atomic force microscope (AFM) to evaluate surface properties of materials and devices with an atomic-sized resolution on a microscopic scale.

We have been studying material characterization with the ultrasonic micro-spectroscopy (UMS) technology [1] using ultrasonic focused waves and ultrasonic plane waves in the VHF and UHF ranges. The UMS technology, in which the line-focus-beam (LFB) acoustic microscopy system [2] plays a central role, analyzes and evaluates material properties through nondestructive, noncontact imaging with a high spatial resolution and/or highly quantitative measurements of the acoustic properties of the materials investigated.

LFB acoustic microscopy can measure the propagation characteristics, viz., phase velocity and attenuation, of LSAWs on the boundary between a solid specimen and the water couplant by $V(z)$ curve measurements. A distinct feature of this system is the perfect directionality of the linearly focused ultrasonic beam, which enables exciting and propagating LSAWs along one desired direction on the water-loaded specimen surface and quantitatively characterizing elastic and structural anisotropy of the specimens

Manuscript received December 4, 2000; accepted July 3, 2001. This work was supported in part by the Research Grants-in-Aid from the Ministry of Education, Science, Sports, and Culture of Japan; the Japan Society for the Promotion of Science for the Research for the Future Program; and the Mitsubishi Foundation.

The authors are with the Department of Electrical Engineering, Tohoku University, Sendai 980-8579, Japan (e-mail: kushi@ecei.tohoku.ac.jp).

with very high accuracy. The system is applicable for specimens of all configurations, such as semi-infinite specimens, thin film or diffused layer specimens, and thin plate specimens. Its applications can be extended to almost all research problems associated with elastic properties of materials, viz., characterization of anisotropy and inhomogeneity in materials; structural analysis of polycrystalline materials; evaluation of thin film, diffused/implanted, or surface-damaged layers; analysis of residual stress and deformation; and determination of the elastic constants of bulk and thin film materials. The system has been applied to a great variety of material characterizations and has been shown to be very useful and effective in evaluating materials and device fabrication processes [1]–[22].

Considerable effort has been made to improve the measurement accuracy of the LFB acoustic microscopy system so that very slight variations or differences in elastic properties of materials can be obtained. The measurement accuracy depends mainly upon the displacement accuracy of the mechanical translation stages of the system and the stability of the temperature environment. The complete system has been installed in a temperature-controlled room so that it achieves a relative accuracy for LSAW velocity measurements to better than ±0.005% at a single chosen point of a specimen and ±0.01% over a scanning area of 75 mm×75 mm [23]. A system calibration method for the absolute measurement has also been proposed to calibrate the differences of measured values of LSAW propagation characteristics resulting from different systems and/or devices used and different ultrasonic frequencies employed [24].

In this paper, we describe a new version of the LFB-UMC system that has been developed from the viewpoint of applying the UMS technology to deal with various problems currently arising in the research and development of materials. The keys to enhancing the accuracy of the system are chiefly the development of stable electrical circuits and a high precision mechanical system, the stabilization of the measurement temperature environment, and the precise temperature measurement of the water couplant. Details of the newly constructed LFB-UMC system and its performance are fully described herein.

II. Measurement Principle

The general measurement principle and the method of LFB acoustic microscopy have been described in detail previously [2]. LFB acoustic microscopy measures the propagation characteristics of LSAWs excited on a water-loaded specimen surface by analyzing the $V(z)$ curves, which are the transducer outputs recorded by changing the distance z between the LFB ultrasonic device and the specimen, as illustrated in Fig. 1. The origin of the coordinate system is placed at the focal plane in water. Ultrasonic plane waves are produced by the transducer and converge into the shape of a wedge, namely the LFB, formed by the cylindrical ultrasonic lens. When the ultrasonic line-

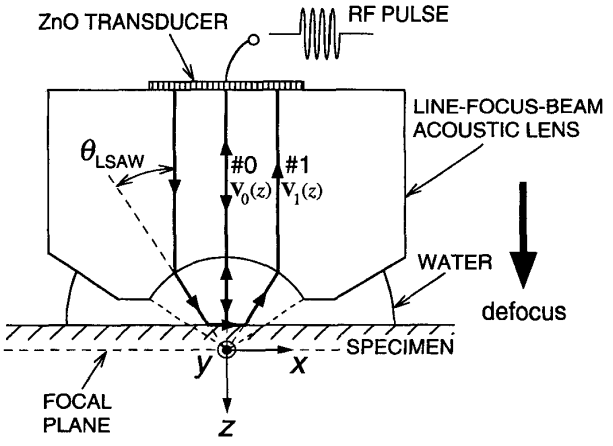

Fig. 1. Cross-sectional geometry of the LFB ultrasonic device describing the principle of $V(z)$ curve measurements.

focused waves are focused onto the surface of the specimen through the water couplant, the component incident at a critical angle θ_{LSAW} excites LSAWs on the water-loaded specimen surface. The LSAWs radiate longitudinal waves into the water at the angle of θ_{LSAW}, propagating on the surface of the specimen. When the ultrasonic device is moved toward the specimen (away from the focal plane), only the two phasor components, viz., axial waves (#0, $\mathbf{V}_0(z)$) and LSAWs (#1, $\mathbf{V}_1(z)$) shown in Fig. 1, effectively contribute to the transducer output because of the effect of the lens [25]. Each phasor is expressed as follows:

$$\mathbf{V}_0(z) = |\mathbf{V}_0(z)| \exp\{j(-2k_W z + \phi_0)\}, \tag{1}$$

$$\mathbf{V}_1(z) = |\mathbf{V}_1(z)| \exp[j\{(-2k_W \cos\theta_{\mathrm{LSAW}})z + \phi_1\}], \tag{2}$$

and

$$k_W = 2\pi f / V_W \tag{3}$$

where $\theta_{\mathrm{LSAW}} = \sin^{-1}(V_W/V_{\mathrm{LSAW}})$; k_W and V_W are the wave number and longitudinal velocity of water, respectively; V_{LSAW} is the LSAW velocity; f is the ultrasonic frequency; and ϕ_0 and ϕ_1 are the initial phases. The output $\mathbf{V}(z)$ curve is obtained as the sum of these two phasors, given by the following equation:

$$\mathbf{V}(z) = \mathbf{V}_0(z) + \mathbf{V}_1(z). \tag{4}$$

Therefore, the amplitude of the phasor $\mathbf{V}(z)$ is expressed as

$$V(z) = |\mathbf{V}(z)| = |\mathbf{V}_0(z) + \mathbf{V}_1(z)|. \tag{5}$$

Fig. 2 shows a typical $V(z)$ curve measured at 225 MHz for a (111) gadolinium gallium garnet (GGG) specimen with LSAWs propagating in the $[\bar{1}\,\bar{1}\,2]$ direction ((111)-$[\bar{1}\,\bar{1}\,2]$ GGG specimen). The LSAW velocity V_{LSAW} is determined from the oscillation interval Δz of the $V(z)$ curve

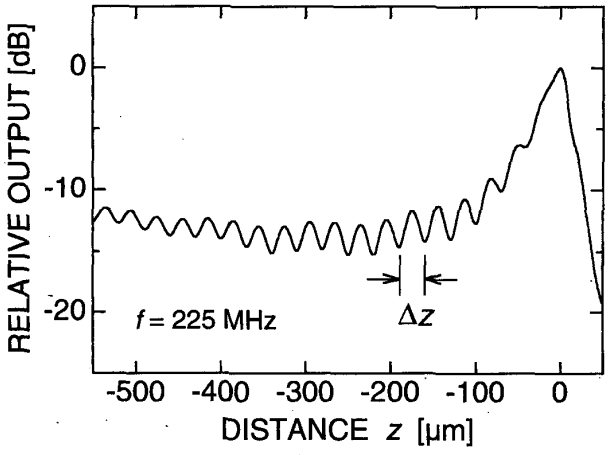

Fig. 2. V(z) curve measured for (111)-[$\bar{1}\,\bar{1}$ 2] GGG specimen at 225 MHz.

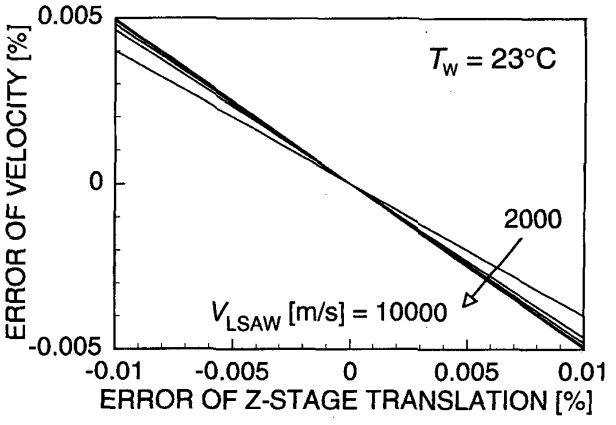

Fig. 3. Numerical calculations of measurement errors of LSAW velocity versus errors of z-stage translation. T_W = 23°C; f = 225 MHz; V_{LSAW} = 2000, 3000, 4000, 6000, and 10 000 m/s.

using the following equation:

$$V_{\mathrm{LSAW}} = \frac{V_W}{\sqrt{1-\left(1-\frac{V_W}{2f\Delta z}\right)^2}}. \tag{6}$$

The attenuation of LSAW is also obtained from the amplitude variation of the V(z) curve. Details of V(z) curve analysis to obtain the LSAW propagation characteristics have been described previously [2].

III. Error Factors

In this section, we discuss the source of errors in measuring the propagation characteristics of LSAWs by LFB acoustic microscopy, focusing on the LSAW velocity, which is used mainly in material characterization. It is easily seen from (6) that the measurement accuracy of the LSAW velocity depends greatly upon three factors: the oscillation interval of the V(z) curve Δz, the longitudinal wave velocity in water V_W, and the ultrasonic frequency, f. The system frequency is sufficiently stable so that the frequency f exhibits no influence on the measurement accuracy. As a consequence, the effects of the displacement errors of the mechanical translation z-stage and the effects of the measurement errors of the water temperature, which involve the parameters of Δz and V_W, respectively, on the measurement accuracy, are treated.

A. Errors of the z-Stage Translation

The translation errors of the z-stage directly affect the intervals Δz of the measured V(z) curves. Although the moving characteristics of the z-stage vary with its moving region in a complicated manner, numerical calculations were made on the assumption that the translation errors occur at a constant rate. Fig. 3 shows the LSAW velocity errors as a function of the translation errors of the z-stage, calculated at 23°C and at 225 MHz according to (6), in the range 2,000 to 10 000 m/s. When the translation error is positive, i.e., when the z-stage travels too far, the measured Δz is too small, and the LSAW velocity obtained is less than the true value. When the translation error is negative, the LSAW velocity obtained is greater than the true value. The slopes are nearly equal at any value of LSAW velocity considered. The reproducibility of the moving characteristics of the z-stage must be ±0.004% to achieve the desired relative accuracy of the LSAW velocity of ±0.002%.

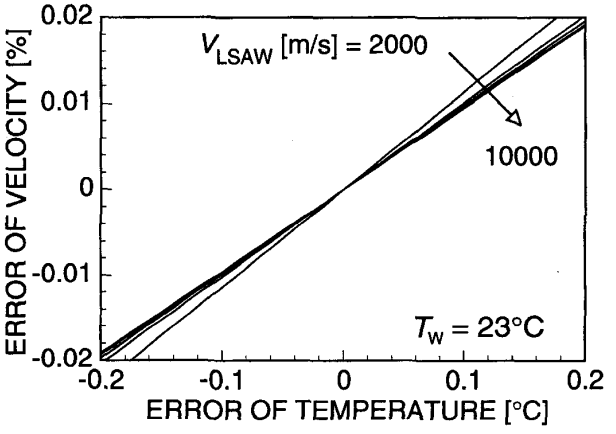

Fig. 4. Numerical calculations of measurement errors of LSAW velocity versus measurement errors of couplant temperature around 23°C. f = 225 MHz; V_{LSAW} = 2000, 3000, 4000, 6000, and 10 000 m/s.

B. Measurement Errors of the Couplant Temperature

In the V(z) curve analysis, the propagation characteristics of LSAWs are obtained using the propagation characteristics of longitudinal waves in water as the reference. The phase velocity V_W and the attenuation coefficient α_W

of longitudinal waves in water are obtained from the literature [26], [27], respectively. Errors in measuring the water temperature directly affect the measurement accuracy of LSAW propagation characteristics. A thermocouple is used to measure the temperature of the water couplant. In general, a temperature distribution exists in the couplant, mainly because of the temperature gradient produced by the temperature decrease at the air surface of the couplant resulting from the heat of vaporization and because of the changes in the temperature of the convective environment around the couplant.

Fig. 4 shows the calculated velocity errors caused by errors in measuring the water temperature using (6) at 225 MHz in the velocity range 2,000 to 10 000 m/s, where the true water temperature value was assumed to be 23°C. When the measured water temperature is greater than the true value, V_W is estimated to be greater, so that the obtained LSAW velocity becomes greater than its true value. The slopes are also nearly equal at any value of the LSAW velocity considered. The measurement accuracy of the water temperature must be better than ±0.02°C to achieve the measurement accuracy of the LSAW velocity of ±0.002%.

IV. LFB-UMC System

The block diagram of the newly developed LFB-UMC system is shown in Fig. 5. The entire system is installed in a temperature- and humidity-controlled clean room. The system consists of eight main elements: the LFB ultrasonic device, pulse-mode measurement system, mechanical system, temperature control system, temperature measurement system, pure water supply system, sample loader and unloader, and computer system.

The system operates in the frequency range of 50 to 1,000 MHz using several ultrasonic devices with different frequency ranges. Experiments in this paper are conducted using an LFB ultrasonic device designed for 225-MHz operation with a cylindrical concave surface of 1-mm radius and an aperture half-angle of 60°, which can be used in the frequency range from 100 to 300 MHz. The pulse-mode measurement system was developed from experience gained from the measurement of radio frequency (RF) tone burst signals [28], [29]. A network/spectrum analyzer (Model HP-4396A with option 1D5 and a custom-made option T01; Hewlett Packard Japan, Ltd.) is used for transmitting and receiving the electrical signals and enables highly accurate measurements of the amplitude and phase of the RF pulse signals in the zero-span mode. The RF pulse signals are applied to the ultrasonic transducer and converted into ultrasonic waves. Only the reflected signal from the surface of the specimen is extracted through the RF gate circuit from the signals reflected from the electrical terminal of the transducer and the lens surface, etc., and fed into the network/spectrum analyzer. In the amplitude measurement, the detected pulse video output is converted into a conventional video output through the peak-holding circuit and low pass filter and is recorded through the 16-bit A/D converter. In the complex mode measurement, the input signals are quadrature-detected and output as the real and imaginary parts of the complex signals. In the V(z) curve measurement, the detected output is precisely recorded as a function of distance z by employing positioning pulses from a laser interferometer for trigger pulses of the A/D converter.

The mechanical system is constructed so that highly accurate measurements are made at a single point on the specimen and over a two-dimensional scanning area. Fig. 6 is a schematic view of the newly developed mechanical system. The z-stage utilizes an air bearing system with precise straightness and is driven by a stepping motor with a harmonic gear and a micro-step driver having a moving resolution of 0.01 μm/step. The straightness of the z-stage is estimated to be better than 1×10^{-7} rad/mm by a laser autocollimator. A laser interferometer using a He-Ne laser (Model 117A; Spectra-Physics Co.) with a resolution of 4 nm is set on the moving axis of the z-stage to determine the position of z accurately. The sample stage is mounted on an automatic three-axis tilting stage placed on the rotation stage. The three-axis tilting stage can provide tilt in the x and y axes and can move in the z-axis direction using stepping motors with resolutions of 6×10^{-7} rad/step and 0.07 μm/step, respectively, enabling alignment between the LFB ultrasonic device and the specimen with the desired accuracy and reproducibility. The scanning range of the xy-stage is 200 mm × 200 mm, enabling measurements for substrates with 200-mm diameter. The rotation and xy-stages are also driven by stepping motors with resolutions of 0.01°/step and 0.1 μm/step, respectively.

The temperature control system is composed of an acrylic chamber with a high efficiency particulate air (HEPA) filter, mounted in its ceiling, and an air conditioning unit, as illustrated in Fig. 7, which houses the mechanical system, including the ultrasonic device and the sample stage. The temperature inside the chamber can be set at a desired value in the range from 19 to 27°C with the temperature controller set in 0.001°C steps. Temperature is measured by a temperature sensor employing a platinum resistance thermometer and is fed into the temperature controller. The air, the temperature of which is controlled by the air conditioning unit, is supplied to the chamber from the upper part through the air supply duct and the HEPA filter by the circulating fan. The return air passes through the air return duct at the lower part of the chamber back to the air conditioning unit. The return air is then cooled by the cooling unit and reheated by the electric heater, whose output is PID-controlled by the temperature controller so that the temperature around the sensor is maintained at the selected value.

During the V(z) curve measurement, the couplant temperature is measured using a copper-constantan thermocouple (JIS T-Model, Class 1; CHINO Co.). A thermoelectric temperature-compensating device [Model ZERO-CON (ZC-114/ZA-10); Komatsu Electronics Inc.] with a stability of better than ±0.005°C is used for the reference (cold) junction of the thermocouple. This temperature measure-

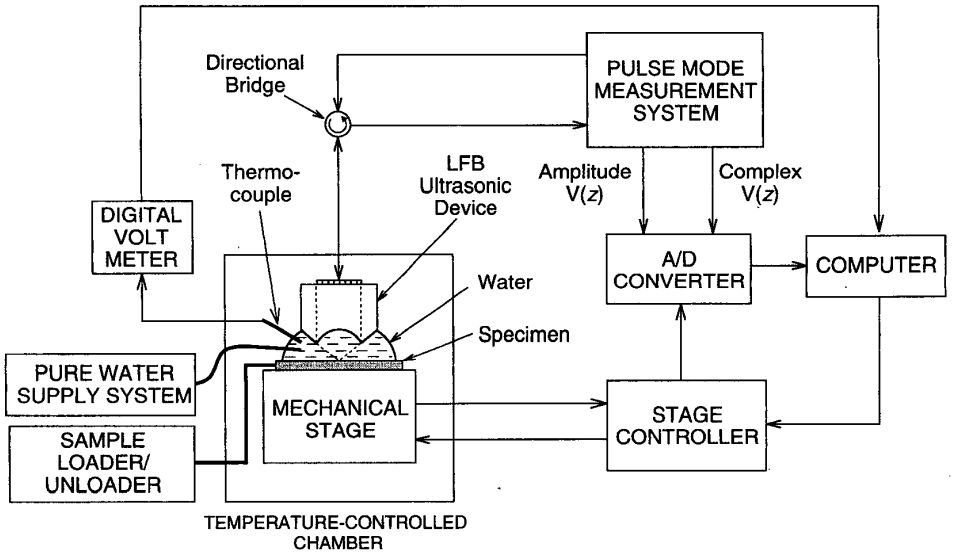

Fig. 5. Block diagram of the LFB-UMC system.

ment system is calibrated within ± 0.01°C using a standard platinum resistance thermometer (Model R800-2; CHINO Co.). An average temperature calculated from eight temperatures taken during one $V(z)$ curve measurement is employed.

The computer controls the entire system and analyzes the measured $V(z)$ curves according to the procedure of $V(z)$ curve analysis [2].

The system is also equipped with a sample transfer system and a temperature-controlled automatic pure water supply system for the couplant to enable measurement of a large number of specimens precisely and efficiently. The details of these systems have been described elsewhere [30].

V. System Evaluation

A. z-Stage

In the previous LFB systems [2], [23], the z-stage positioning was determined by counting the number of pulses of the stepping motor drivers. The translation accuracy of the mechanical stages depends on the mechanical precision of their components, such as lead screws and guides, and the rotation accuracy of the stepping motors and harmonic gears; hence, the moving characteristics of the stages vary with their travel regions and are not always uniform. Therefore, high reproducibility of LSAW velocity measurements can be realized by using the same travel region of the z-stage in $V(z)$ curve measurements [23], [24]. However, the moving characteristics of the mechanical stages may change with time because of friction heat and wear of their mechanical components. To avoid these effects, the distance z is determined by the method described in the Section IV (i.e., a laser interferometer).

The usefulness of this method is discussed here by comparing the positioning accuracy with that obtained by the conventional method using the number of pulses for the stepping motor. In examining the positioning accuracy of the z-stage, we used the previously developed method of measuring the moving characteristics of precision mechanical translation stages using ultrasonic plane waves [31]. In this method, the LFB ultrasonic device in the system is replaced with a plane wave ultrasonic device to radiate plane waves through a water couplant onto a reflector set on the z-stage. The moving characteristics of the z-stage are investigated by measuring and analyzing the phase variation of the signals reflected from the reflector with the z-stage translation. Ultrasonic plane waves at 200 MHz were used in the measurements, and the travel distance of the z-stage was selected to be 600 μm, considering the measurement conditions of the $V(z)$ curve using the LFB ultrasonic device designed for 225-MHz operation.

Fig. 8(a) shows the measured relative phase variations for the distance z positioned by the pulse number for the stepping motor, where the phase changes caused by propagation of longitudinal waves in water were subtracted from the measured phases. Hence, the relative phase variations reflect the positioning characteristics of the z-stage. The phase velocity of the longitudinal waves in water was found to be 1491.23 m/s at 23°C from the literature [26], and the wavelength was calculated to be 7.46 μm at 200 MHz. Hence, the phase changes by 360° for a z-stage translation of 3.73 μm, and a phase change of 1° corresponds to a z-stage translation of about 0.01 μm. Periodic changes of approximately 10°, corresponding to the z-stage translation of 0.1 μm, at intervals of 40 μm for z are observed in Fig. 8(a). These are attributed to the harmonic gear used for driving the z-stage. Fig. 8(b) shows the positioning characteristics of the z-stage positioned by the laser in-

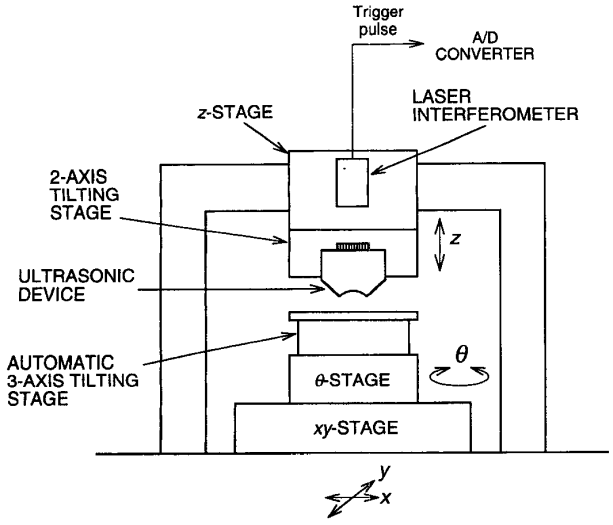

Fig. 6. Schematic view of the mechanical system.

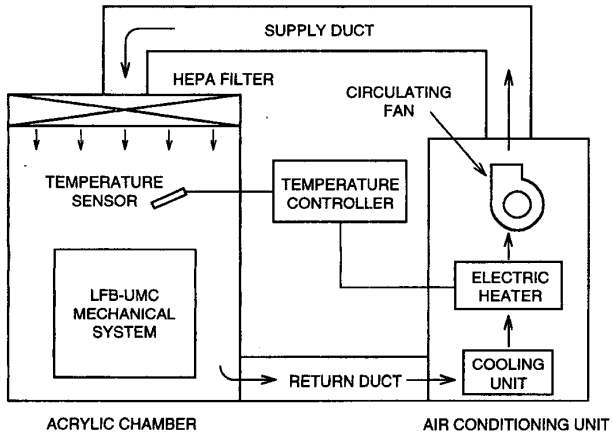

Fig. 7. Schematic view of the temperature control system.

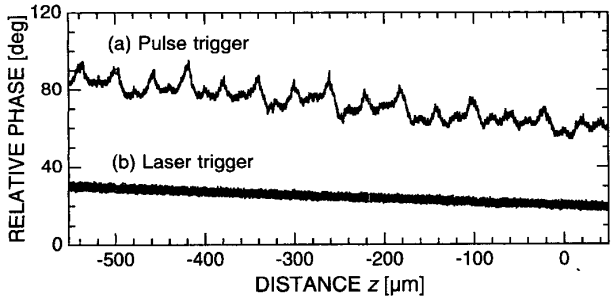

Fig. 8. Positioning errors of the z-stage with the number of pulses for stepping motor (a) and with the laser interferometer (b).

terferometer. Although small variations of approximately 4° are detected, it is found that the periodic changes shown in Fig. 8(a) are completely eliminated and that highly accurate positioning is accomplished.

The measured relative phases both in Fig. 8(a and b) have a negative gradient with respect to z over the entire travel region. Although the positioning errors of the z-stage or misalignment between the ultrasonic device and the reflector could cause this, the primary cause may be the measurement error of the couplant temperature because there is a temperature difference between the propagation region of the ultrasonic waves and the temperature measurement position caused by the temperature distribution in the couplant, as described in the Section III-B. Hence, the phase variation caused by wave propagation in water with no translation error of the z-stage is not correctly subtracted because of the erroneous estimation of the longitudinal wave velocity of water using the measured temperature. If the gradient of the relative phase shown in Fig. 8(b) is assumed to be caused by temperature measurement errors, the temperature difference in water is estimated to be 0.096°C. This temperature distribution in the water couplant will be discussed in the Section V-C.

B. Alignment

Alignment between the LFB ultrasonic device and the specimen surface is of fundamental importance for reliable, accurate measurements. The alignment can be made with high accuracy and high reproducibility using two tilting stages, with the ultrasonic device mounted on one and the sample stage mounted on the other, as shown in Fig. 6. However, there might still be some problems because of the yaw and pitch of the z-stages during the V(z) curve measurements and because of the roll and pitch of the xy-stages and the surface profile of the specimen in two-dimensional measurements. Hence, we investigated the influences of misalignment on the measurement accuracy of the LSAW velocity by performing experiments at 225 MHz for the (111)-[$\bar{1}\,\bar{1}$2] GGG specimen.

Because the LFB acoustic lens has a cylindrical surface, we conducted experiments for the two cases shown in Fig. 9, which depicts the experimental situations for the specimen surface tilted along the focused and unfocused axes of the lens. Fig. 10 shows the changes of the relative output of the signal, reflected from the specimen surface placed at the focal plane, for the tilting angle φ. Circles represent the results for case a, and dots for case b in Fig. 9. The relative output of the reflected signal barely changed when the specimen was tilted along the focused axis in the experimental range, but changed significantly when the specimen was tilted along the unfocused axis. Hence, highly accurate alignment can be made by utilizing the tilting angle dependence of the output along the unfocused axis of the reflected signal. Conversely, the tilting of the specimen surface along the unfocused direction, i.e., misalignment, can be estimated using the output change.

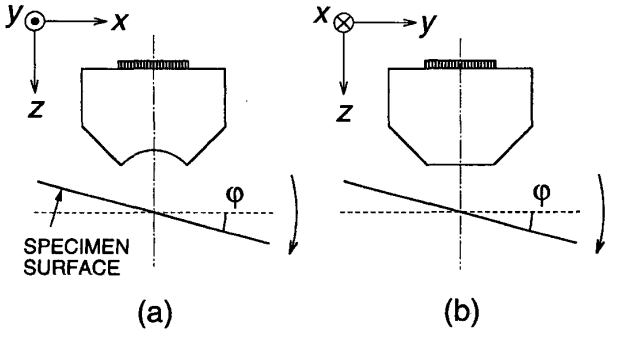

Fig. 9. Schematic views of two cases of misalignment. The specimen is tilted along the focused direction (a) and unfocused direction (b).

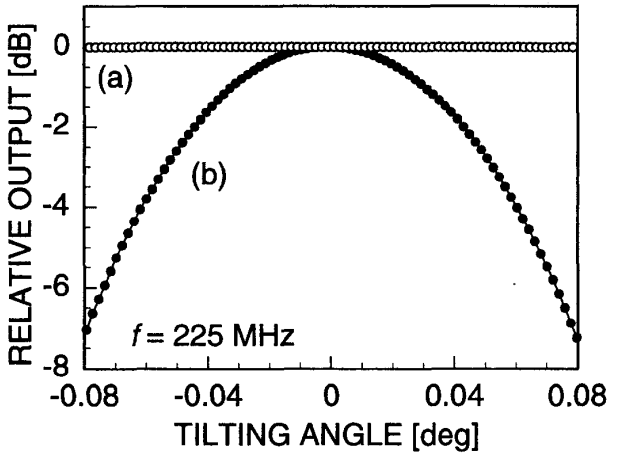

Fig. 10. Changes of output of reflected signal for the tilting angle of the specimen placed at the focal plane. Circles represent the results for case (a) shown in Fig. 9, and dots represent the results for case (b).

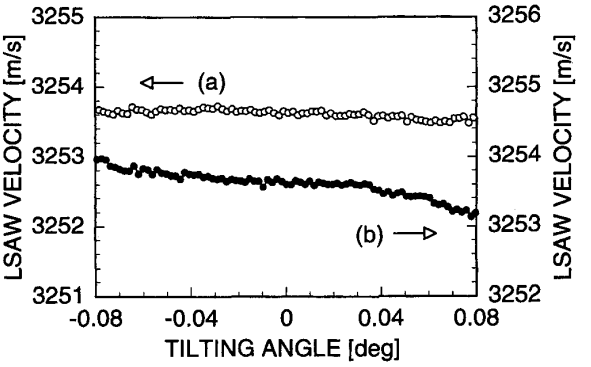

Fig. 11. Measured results of LSAW velocity changes versus tilting angles. Circles represent the results for case (a) shown in Fig. 9, and dots represent the resuls for case (b).

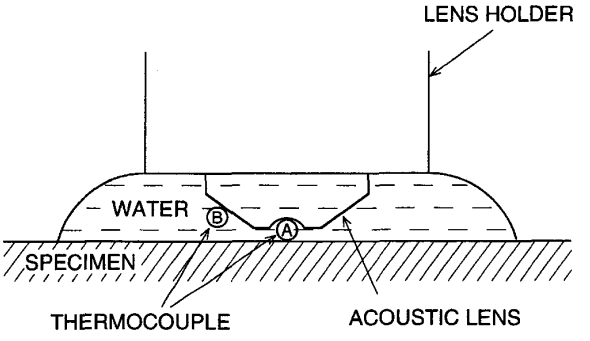

Fig. 12. Schematic view of measuring temperature distribution in water couplant using two thermocouples.

The results of the influence of misalignment on the LSAW velocity measurements are shown in Fig. 11(a and b), which correspond to cases a and b of Fig. 9. It is observed that misalignment must be within ±0.03° for both the cases to guarantee a velocity measurement accuracy within ±0.002%. Better alignment within ±0.01° along both the focused and unfocused axes should be made for precise measurements, as the tilting stages used in the present system have sufficient resolution and reproducibility for such precise alignment as described in Section IV. The profile of the measured values in case b, shown in Fig. 11(b), does not exhibit symmetry for the tilting angle. This might be due to the thickness distribution and inhomogeneity of the ZnO film for the transducer and the acoustic matching layer on the cylindrical lens surface or anisotropy of the sapphire LFB lens. Therefore, it is necessary to examine the influence of the misalignment on velocity measurements for each device used in the system in advance, as different characteristics could exist among employed ultrasonic devices.

C. Temperature Distribution in the Water Couplant

The measured temperature using a thermocouple during the V(z) curve measurements differs from the temperature of the propagation region of the ultrasonic waves, because of the temperature distribution in the water couplant, as described in Section III-B. This causes some errors in determining the longitudinal wave velocities of the water couplant used for determination of V_{LSAW} given in (6). We therefore investigated the temperature distribution in the couplant at two positions using two thermocouples, as shown in Fig. 12. One thermocouple was positioned just under the LFB lens surface, denoted as region A, where the ultrasonic focused waves propagate for actual V(z) curve measurements and the thermocouple cannot be placed. The other was positioned near the lens surface, denoted as region B, where the water temperature is usually measured during V(z) curve measurements. The temperature in region A, T_A, and that in region B, T_B, are measured simultaneously when the temperature distribution in the couplant is stable, and the temperature difference between two regions, ΔT, is given by

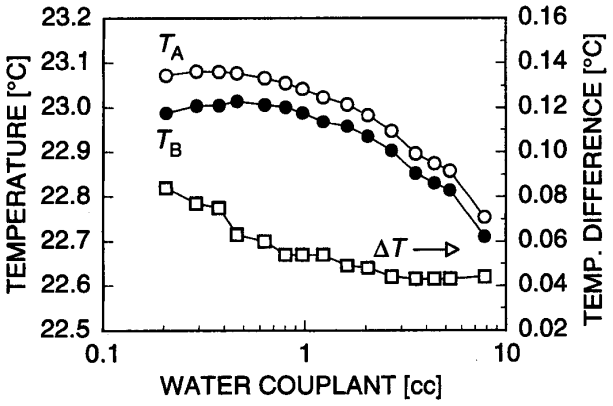

Fig. 13. Dependences of temperatures T_A and T_B and temperature difference ΔT in water couplant on volume of the couplant.

$$\Delta T = T_A - T_B. \tag{7}$$

The temperature distribution was investigated for an LFB ultrasonic device designed for 225-MHz operation, which is usually employed for material characterization by the LFB-UMC system. The distance between the two thermocouples was approximately 3 mm, and the distance between the lens surface and the specimen was the focal length of 1.15 mm in region A. The xy-stage used in the system was set at the origin ($x = y = 0$) of the system coordinate. The entire mechanical system, including the specimen, was installed in a temperature-controlled chamber in which the relative humidity was within $40 \pm 1\%$ during the measurements.

First, the relationship between the temperature distribution and the quantity of the couplant was studied using the GGG substrate as the specimen. The measured temperatures T_A and T_B are given in Fig. 13. Each of the plotted values is the average of 10 measurements exhibiting a maximum deviation of ± 0.01°C. T_B is less than T_A, because of the vaporization heat of water. As the couplant quantity increased, both T_A and T_B decreased monotonically. The increase of the surface area of the water couplant, facing the air, probably helped to increase the total heat of the water vaporization. The obtained values of ΔT are also given in Fig. 13, where it is seen that ΔT became larger as the couplant quantity decreased. When the couplant volume was in the range from 0.6 to 1.2 cc for the present system, the values of ΔT were within 0.057 ± 0.003°C, corresponding to a measurement error of $-0.0057 \pm 0.0003\%$ in LSAW velocity from the previous numerical calculation using (6).

Next, the relationship between the temperature difference and the thermal conductivity of materials was investigated using a couplant quantity of 0.7 cc. We examined many specimens, such as Teflon; Pyrex glass; single crystal plates of $LiTaO_3$, $LiNbO_3$, α-quartz, GGG, and Si; and metal plates of Al and Au, with different thermal conductivities and thicknesses. The results are shown

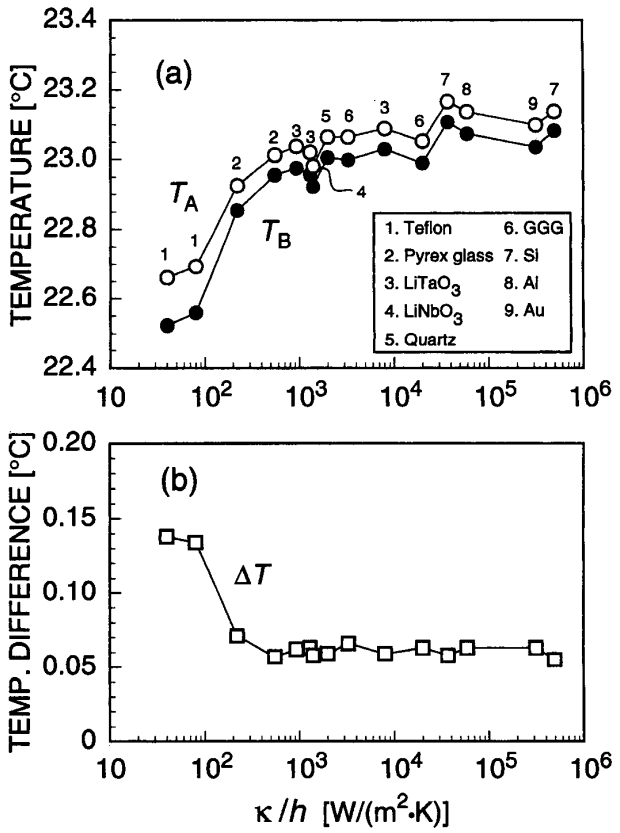

Fig. 14. Dependences of temperatures T_A and T_B (a) and temperature differences ΔT (b) in water couplant on thermal conductivities κ of specimens with couplant volume of 0.7 cc. The thermal conductivity is divided by the specimen thickness h.

in Fig. 14, where thermal conductivity κ/h is used considering the thicknesses of the specimens. The temperature was greater for specimens with larger thermal conductivity, as shown in Fig. 14(a). ΔT was the greatest for the smallest thermal conductivity, as shown in Fig. 14(b). The values of ΔT were within 0.063 ± 0.008°C, corresponding to a measurement error of $-0.0063 \pm 0.0008\%$ in LSAW velocity, for specimens such as single crystals, glasses, and metallic materials, which are usually characterized by the LFB-UMC system and have thermal conductivities exceeding 2×10^2 W/(m$^2 \cdot K$).

Similarly, the temperature difference was also measured for the ultrasonic plane wave device used to evaluate the z-stage moving characteristics in Section V-A. The difference was 0.094°C, which was in good agreement with the value of 0.096°C estimated from the phase gradient shown in Fig. 8.

VI. Measurement Procedure

A. Water-Couplant Temperature

For the V(z) curve measurements at a single chosen point, the temperature T_A during measurement is deter-

mined accurately using T_B and ΔT according to the relationship

$$T_A = T_B + \Delta T \tag{8}$$

where T_B is measured during the period of $V(z)$ curve measurements using the thermocouple and ΔT is obtained in advance for each specimen under the same stable conditions as $V(z)$ curve measurements at a single point on the specimen surface.

For two-dimensional measurements, the values of ΔT could, in general, be different at different positions on the specimen surface. Therefore, a method of determining the water temperature and the longitudinal wave velocity in water was developed using $V(z)$ curves to obtain the longitudinal wave number in water, k_W.

A carrier leakage signal, denoted by V_e, arises from an insufficient on/off ratio in the RF tone burst pulse generation circuit used in the system. The phasor $\mathbf{V}_e$ does not depend on the relative distance z and is approximately expressed as

$$\mathbf{V}_e = |\mathbf{V}_e| \exp(j\phi_e) \tag{9}$$

where ϕ_e is the phase. The $\mathbf{V}_e$ signal is received and detected together with the $V(z)$ curve signal. Fig. 15(a) shows the typical $V(z)$ curve measured for the (111)-[$\bar{1}\bar{1}$2] GGG specimen at 225 MHz. The on/off ratio of the RF pulse generation circuit was 75 dB. Small interference signals between the $V(z)$ curve signals and the V_e signals exist over the entire $V(z)$ curve. The interference signals are derived from the $V(z)$ curve as shown in Fig. 15(b). The spectral distribution of the interference signals from $z = -500$ to -30 μm in Fig. 15(b) was obtained by FFT analysis as shown in Fig. 15(c). The two peaks in the spectral distribution correspond to the wave numbers $k_0 (= 2k_W)$ and $k_1 (= 2k_W \cos\theta_{\mathrm{LSAW}})$, which are associated with phasors $\mathbf{V}_0$ and $\mathbf{V}_1$, determining the $V(z)$ curves, as given by (1) and (2), respectively. Therefore, k_W was successfully obtained from $k_W = k_0/2$. Fig. 2 shows the $V(z)$ curve from which the small interference signals were removed. As described in Section IV, the system operates in the complex mode measurement so that k_W can be also obtained from the measured complex $V(z)$ curves.

The wave numbers, however, obtained from the $V(z)$ curves were slightly different from the true value of k_W because of the performance characteristics of the ultrasonic device employed. Therefore, a procedure to measure the water temperature, $T_W(x, y)$, and the longitudinal wave velocity in water, $V_W(x, y)$, at the position (x, y) on the specimen surface in two-dimensional measurements was developed using the wave number, expressed as k'_W, obtained from the $V(z)$ curve.

$T_W(x, y)$ is given using T_{A0} as a reference value obtained at a single point measurement by

$$T_W(x, y) = T_{A0} + \Delta T_W(x, y). \tag{10}$$

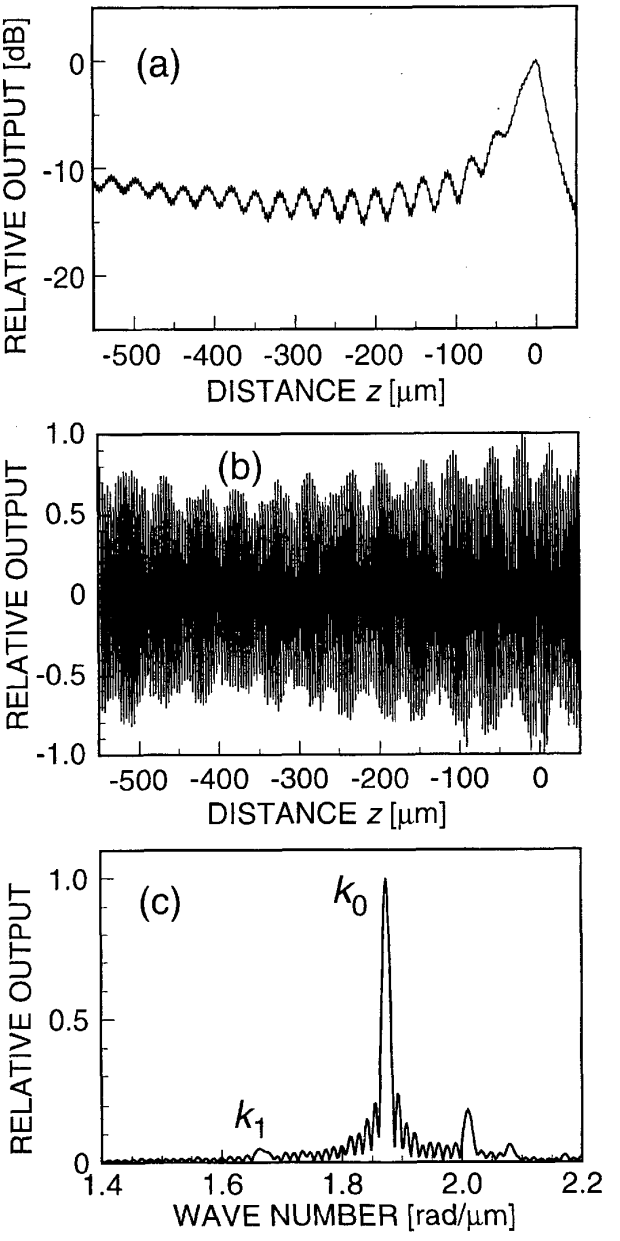

Fig. 15. $V(z)$ curve measured for (111)-[$\bar{1}\bar{1}$2] GGG specimen at 225 MHz and spectral distribution of the small interference signals on the $V(z)$ curve. a) $V(z)$ curve, b) interference signals, and c) spectral distribution.

Because V_W' is equal to $2\pi f/k_W'$, $\Delta T_W(x,\ y)$ is given by

$$\Delta T_W(x,\ y) = \frac{V_W'(x,\ y) - V_{W0}'}{\frac{dV_W'}{dT}} = \frac{2\pi f \cdot \left\{k_{W0}' - k_W'(x,\ y)\right\}}{k_{W0}' \cdot k_W'(x,\ y) \cdot \frac{dV_W'}{dT}} \quad (11)$$

where k_{W0}' at T_{A0} is obtained from the V(z) curves measured at a single point on the specimen surface under stable temperature conditions and $k_W'(x,\ y)$ is obtained from the V(z) curve measured at position (x, y). The changing ratio of V_W' for temperature is obtained from the literature [26], as it is nearly equal to that of V_W. $T_W(x,\ y)$ is then obtained by substituting (11) into (10).

Similarly, $V_W(x,\ y)$ is obtained using V_{W0} at T_{A0} as a reference value as

$$V_W(x,\ y) = V_{W0} + \Delta V_W(x,\ y) \quad (12)$$

where $\Delta V_W(x,\ y)$ is represented by

$$\Delta V_W(x,\ y) = \frac{dV_W}{dT} \cdot \Delta T_W(x,\ y). \quad (13)$$

Therefore, if $\Delta T_W(x,\ y)$ is determined, $V_W(x,\ y)$ is obtained by substituting (13) into (12). $\Delta V_W(x,\ y)$ is also given by substituting (11) into (13) as

$$\Delta V_W(x,\ y) = \frac{2\pi f \cdot \left\{k_{W0}' - k_W'(x,\ y)\right\}}{k_{W0}' \cdot k_W'(x,\ y)}. \quad (14)$$

Even for the V(z) curve measurements at a single point, the monitoring of k_W' discussed previously is also useful for understanding and confirming the experimental temperature situations.

B. LSAW Velocity

1. Single Point Measurement: A flowchart of the measurement procedure for obtaining the LSAW velocity at a single point and stable temperature is shown in Fig. 16. First, the V(z) curves are obtained for a standard specimen used for system calibration [24] and for the specimen examined (step S1). T_B should be corrected using the value of ΔT measured in advance (step S4) if the values of ΔT differ between them (step S2). However, it need not be corrected (step S3) if the values of ΔT are the same, but it is necessary to confirm that the analyzed values of k_W' for both specimens are almost constant for precise velocity measurements. Next, the V(z) curve analysis and the calibration method are applied, and V_{LSAW} is obtained for the specimen examined (steps S5 and S6). However, if the values of ΔT for the examined and standard specimens are slightly different, e.g., ± 0.01°C, V_{LSAW} is obtained within the estimated measurement error associated with the temperature, $\pm 0.001\%$, using T_B.

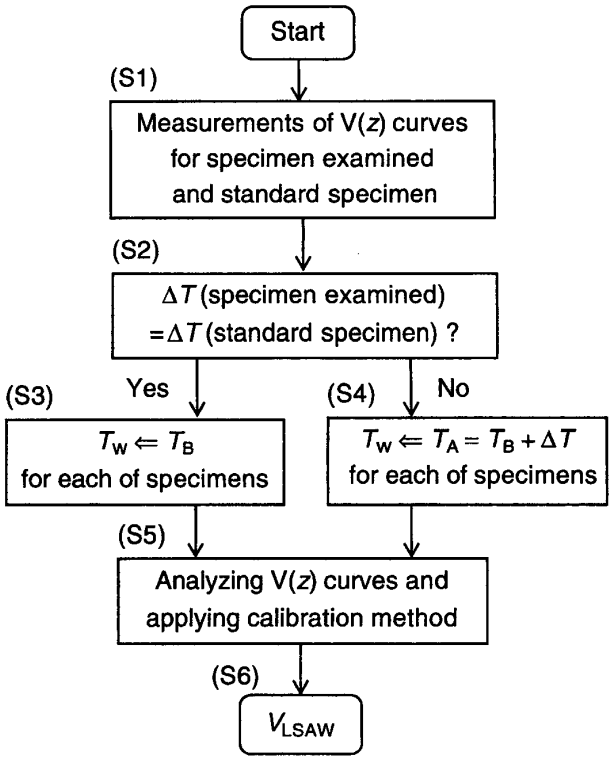

Fig. 16. Measurement procedure of LSAW velocities at a single point.

2. Two-Dimensional Measurement: A flowchart of the procedure for two-dimensional measurements is shown in Fig. 17. T_B measured for the standard specimen should be corrected using ΔT (steps S1 to S3). $T_W(x,\ y)$ and $V_W(x,\ y)$ in two-dimensional measurements for the specimen examined are determined by the proposed method using the V(z) curves (steps S4 to S7). V_{LSAW} is then obtained by analyzing V(z) curves and applying the calibration method (steps S8 to S10). If $\Delta T_W(x,\ y)$ in (10) is small, e.g., ± 0.01°C, V_{LSAW} is obtained within the estimated measurement error associated with the temperature, $\pm 0.001\%$, using T_{A0} as $T_W(x,\ y)$.

VII. Measurements and Results

We investigated the stability of the measurement temperature environment and actual accuracy of the present LFB-UMC system for LSAW velocity measurements at 225 MHz, using two specimens of optical grade Z-cut $LiTaO_3$ and (100) Si single crystal substrates. ΔT for each specimen was obtained from the results in Fig. 14(b). The specimens used have sufficient thickness to avoid the influence of the reflected waves from their back surface on the LSAW velocity measurements [32], [33].

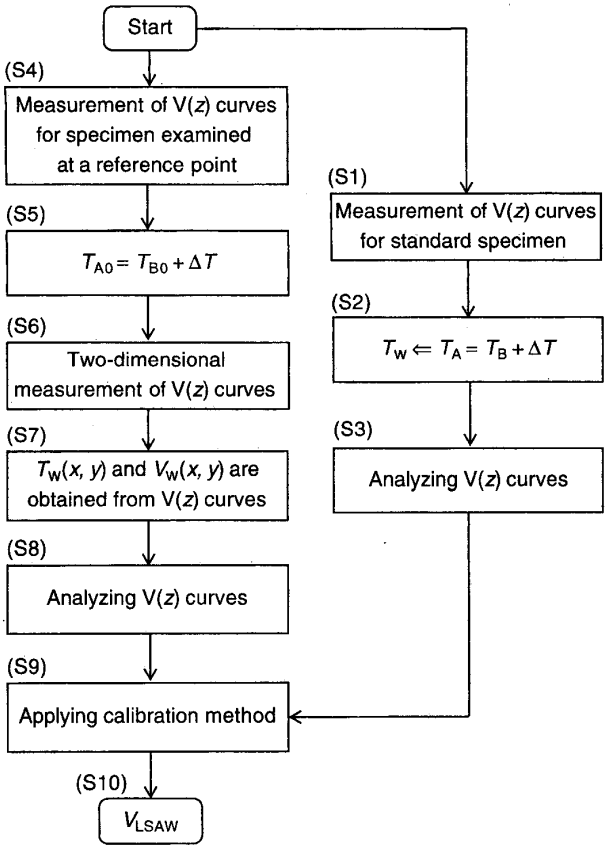

Fig. 17. Measurement procedure of LSAW velocities in two-dimensional measurements.

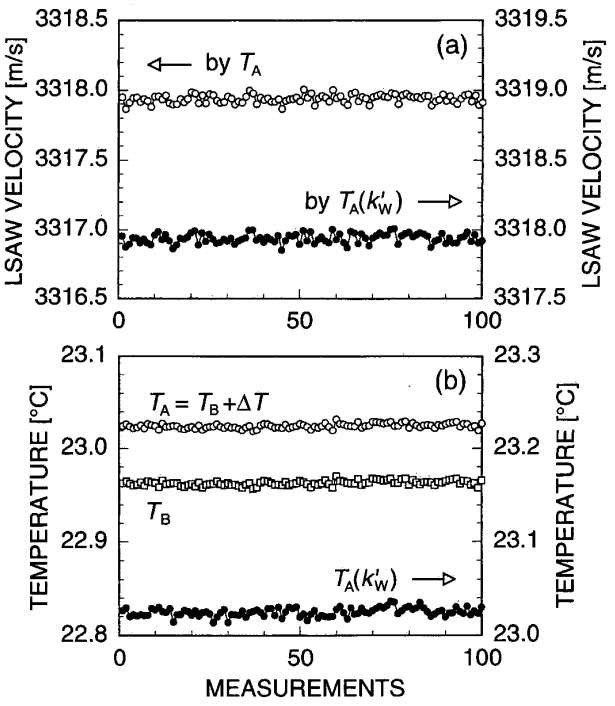

Fig. 18. Experimental results of 100 repeated V(z) curve measurements for ZY-$LiTaO_3$ specimen at 225 MHz. a) LSAW velocities using water couplant temperatures T_A and $T_A(k'_W)$; b) water couplant temperatures T_A, T_B, and $T_A(k'_W)$.

A. Optical Grade $LiTaO_3$ Crystal

Using the measurement procedure shown in Fig. 17, we demonstrated that the LFB system could evaluate the elastic homogeneity of a commercially available, optical grade $LiTaO_3$ single crystal (length: 79 mm; diameter: 101 mm) [34] grown and pulled along the crystallographic Y-axis direction by the Czochralski method. A 4-mm thick Z-cut substrate, prepared in parallel along the pulling Y-axis direction, was taken for LSAW velocity measurements in which LSAWs propagated along the Y-axis direction. The (111)-$[\bar{1}\,\bar{1}\,2]$ GGG specimen was used as the standard specimen for the system calibration [24].

First, following the measurement procedure in Fig. 16, we repeated V(z) curve measurements 100 times (35 min) at the central position of the specimen surface in a well-stabilized measurement temperature environment, to obtain the reference temperature T_{A0}. The water couplant volume was 0.7 cc. Fig. 18(b) shows the water couplant temperatures T_B measured by the thermocouple at region B in Fig. 12 and the determined temperatures T_A obtained from (8) with $\Delta T = 0.062$°C for the 4-mm thick Z-cut $LiTaO_3$ substrate, and, for reference, variations of the "averaged" temperatures $T_A(k'_W)$ on the wave propagation path estimated from the wave numbers k'_W of the longitudinal velocities in the recorded V(z) curves. The measured temperatures, T_B and T_A, were almost constant with some variations during the measurements, similar to the variations in $T_A(k'_W)$. The averaged value of temperature T_A was 23.025°C with $\pm 2\sigma$ of ± 0.005°C, and that for $T_A(k'_W)$ was 23.025°C with $\pm 2\sigma$ of ± 0.009°C, where σ is the standard deviation. The resolution in T_A or T_B is slightly better than that in $T_A(k'_W)$. However, a very stable temperature environment was maintained for long-time measurements because of the temperature controller used in the system. Further stabilization of the temperature environment is possible by enclosing the specimen area and by circulating precisely temperature-controlled water around the enclosed area. The calibrated LSAW velocities determined using the values T_A and $T_A(k'_W)$ and the oscillation intervals Δz analyzed from the V(z) curves are shown in Fig. 18(a). The averaged LSAW velocity is 3317.94 m/s with $\pm 2\sigma$ of ± 0.06 m/s ($\pm 0.0018\%$) for T_A and with $\pm 2\sigma$ of ± 0.07 m/s ($\pm 0.0021\%$) for $T_A(k'_W)$. T_{A0} was taken as 23.025°C.

Next, we measured the V(z) curves in 1-mm steps over a distance of 66 mm on the specimen surface along the x axis of the system (along the central line of the Y axis of the Z-cut substrate), where the y stage was set at the origin ($y = 0$). Temperatures $T_B(x)$ measured using the thermocouple during V(z) curve measurements are plotted as dots

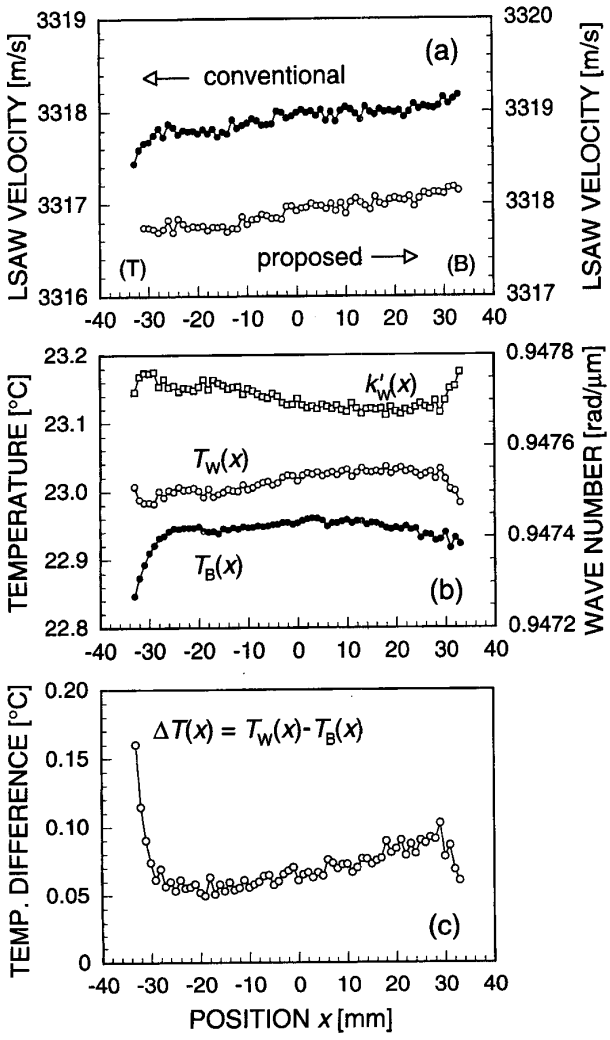

Fig. 19. Correction of LSAW velocity variations measured for ZY-$LiTaO_3$ substrate. a) LSAW velocities, b) water couplant temperatures $T_W(x)$ and $T_B(x)$ and longitudinal wave number $k'_W(x)$, and c) $\Delta T(x) = T_W(x) - T_B(x)$.

in Fig. 19(b). $T_B(x)$ rapidly decreased for $x < -25$ mm, near the edge of the specimen, because the thermocouple was set at the left side of the lens surface in water and the maximum deviation was 0.114°C. V_{LSAW} determined using V_W obtained from the literature [26] using the values of $T_B(x)$ is plotted as dots in Fig. 19(a), where the velocities are calibrated with the GGG standard specimen. V_{LSAW} decreased rapidly for $x < -25$ mm, as did $T_B(x)$.

$k'_W(x)$, obtained from the measured V(z) curves, and $T_W(x)$, obtained from (10) and (11), are also shown in Fig. 19(b). An average value of 23.013°C and a maximum deviation of 0.053°C were obtained for $T_W(x)$. The deviation of $T_W(x)$ was less than that of $T_B(x)$, which shows that the temperature at region A was more stable than that at region B. Fig. 19(c) shows the temperature differences $\Delta T(x)$ between $T_W(x)$ and $T_B(x)$ in Fig. 19(b). With the x-stage translation, $\Delta T(x)$ exhibits a maximum temperature variation of 0.110°C from the minimum 0.050°C at $x = -19$ mm to the maximum 0.160°C at $x = -33$ mm and has relatively greater changes around both ends in the measured region. The calibrated LSAW velocities obtained using $T_W(x)$ are also plotted as circles in Fig. 19(a). The true values of LSAW velocities of the specimen were successfully determined with a maximum deviation of 0.49 m/s and increased almost monotonically from the top to the bottom of the crystal substrate. The LSAW velocity increase corresponds to the increase in the chemical composition ratio of 0.016 Li_2O-mol% [34]. This information can be used to improve the crystal growth conditions, e.g., chemical composition ratio of the starting material, for obtaining more homogeneous crystals.

The results just presented suggest that it is of primary importance for accurate measurements to properly and correctly detect the temperature variations during the measurements; in the measurement principle presented in (6), a slight measurement error in temperature, e.g., ±0.05°C, results in a determined LSAW velocity error of ±0.005%. The results also suggest that the temperature correction method using k'_W is very effective when the temperature variations exceed ±0.01°C. However, we have to recognize that there is no serious dependence of the theoretical water-loading effect on the Z Y-$LiTaO_3$ substrate [i.e., the velocity change of ±0.007 m/s (±0.0002%) for ±0.05°C from the calculated value of −0.143 m/s/°C around 23°C using the acoustical physical constants of water [26], [35] and $LiTaO_3$ [36], [37]], according to the LSAW analysis procedure by Campbell and Jones [38].

B. Large Diameter Si Substrate

We also conducted two-dimensional measurement of the LSAW velocity for a large diameter substrate using a 3-mm thick, 200-mm diameter (100) Si substrate with LSAWs propagating along the [001] direction as the reference substrate with sufficient elastic homogeneity. A (100) Si standard specimen[1] [39] was used for the system calibration for the present specimen. Fig. 20 shows the LSAW velocities measured at 225 MHz in 1-mm steps over a distance of 180 mm on the diameter of the substrate along the x axis of the system with the measurement procedure described in Section VI-B. The average value of LSAW velocities was 4926.89 m/s with $\pm 2\sigma$ of ±0.19 m/s (±0.0039%). The elastic properties on the substrate surface of the commercially produced Si single crystal should be uniform for the present measurement resolution by the LFB system[2] [40]. Therefore, the results might contain some other slight, additional measurement errors associated with the thermal

[1]We prepared the standard specimens of (111) and (100) Si grown by the CZ and FZ methods. The acoustic properties will be reported elsewhere.

[2]We measured the impurity dependence of P concentration on the LSAW velocities by the LFB-UMC system. The results will be reported elsewhere.

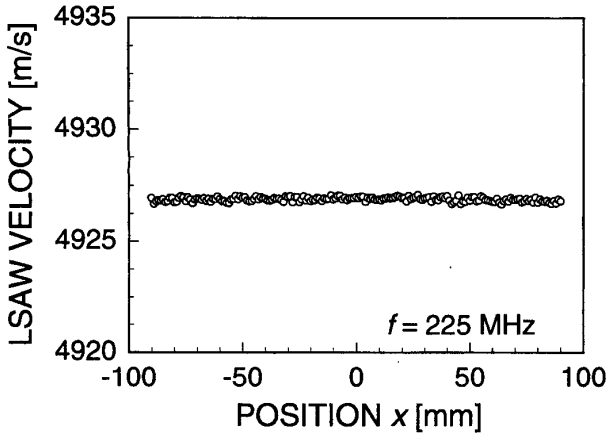

Fig. 20. Measurements of LSAW velocity for (100)-[001] silicon along the diameter of 180 mm at 225 MHz.

fluctuation around the large substrate because measurement resolutions with $\pm 2\sigma$ of $\pm 0.0015\%$ to $\pm 0.0021\%$ were observed for 50 repeated $V(z)$ curve measurements at nine positions separated in 20-mm steps on the scanning line in a stable temperature environment.

VIII. Summary and Further Studies

In this paper, we described a new version of the LFB-UMC system developed for highly accurate detection of slight changes in the physical and chemical properties in and among substrates to resolve scientific and industrial materials problems that have arisen with the recent production of large diameter crystals and wafers.

The effects of translation errors of the z-stage used in the system and measurement errors of the couplant temperature, which are considered to be the main causes of the errors in LSAW velocity measurements, were calculated and discussed based on the measurement principle. To attain a relative accuracy of $\pm 0.002\%$ in the LSAW velocity measurements, the moving accuracy of the z-stage and the measurement accuracy of the water couplant temperature are required to be better than $\pm 0.004\%$ and $\pm 0.02°C$, respectively. We also investigated the temperature distribution in the water couplant and found that the temperature distribution depended on the volume of couplant and on the thermal conductivities of the specimens. A method for correcting the temperature and longitudinal wave velocity of the water couplant was developed, and a measurement procedure to obtain an accurate LSAW velocity at a single chosen point and in two-dimensional measurements was established.

The developed LFB-UMC system was constructed to satisfy these requirements. In investigating the measurement accuracy of LSAW velocities, the system achieved a relative accuracy of better than $\pm 0.002\%$ at any single point and $\pm 0.004\%$ in two-dimensional measurements over a scanning area of 180 mm $\times$ 180 mm. Further improvement of the measurement accuracy could be expected with better stabilization of the temperature environment around the specimen.

Although the discussions in this paper have been about the LSAW velocities obtained by analyzing the amplitude of the $V(z)$ curves, the system is capable of measuring the amplitude and phase of RF tone burst signals with high accuracy so that complex $V(z)$ curves can also be measured. To measure LSAW velocity accurately through the complex $V(z)$ curves, it is essential that the phase variations in the $V(z)$ curve are measured with very high accuracy. Hence, higher translation accuracy of the mechanical system and a more stable temperature environment are required in the complex $V(z)$ curve measurements than in the amplitude $V(z)$ curve measurements. For this reason, it is more suitable to use only the amplitude information of the $V(z)$ curve in practical material analyses and evaluations. However, because the measurement and analysis of complex $V(z)$ curves [41]–[43] are carried out exactly following the construction mechanism of the $V(z)$ curve, the complex $V(z)$ curves are very useful in analyzing the system performance and in studying the measurement models and the causes of measurement errors [31], [42], [44]. This system is also capable of measuring the propagation characteristics of bulk waves by replacing the LFB ultrasonic device with a plane wave ultrasonic device. Elastic constants are determined [5], and standard specimens for the LFB systems are fabricated [24], through the measurements of the bulk wave velocities in solid specimens.

In our future studies, we intend to apply this system to resolve various materials problems in science and industry by developing useful analysis and evaluation methods. Before the temperature correction method established here was introduced, the system was applied to characterizing silica glasses [45], evaluating and selecting $LiNbO_3$ and $LiTaO_3$ wafers for SAW devices [30], [46] evaluating inhomogeneities of optical grade $LiTaO_3$ crystals [34], characterizing and evaluating optoelectronic device fabrication processes such as proton-exchanged layers and domain-inverted layers [47]–[49], and precisely determinating acoustical physical constants of $LiNbO_3$, $LiTaO_3$, synthetic α-quartz, and synthetic silica and fused quartz glasses [36], [45], [50]–[52]. Furthermore, we will utilize the system in studies for improving conventional ultrasonic metrology methods and their accuracy and for developing new methods of measuring the acoustic properties of materials.

Acknowledgments

The authors thank N. Chubachi for his helpful discussions and encouragement throughout this work and T. Sannomiya, N. Akashi, and T. Kobayashi for their invaluable support with the experiments. The authors are very grateful to R. Suganuma (Honda Electronics Co.), M. Hidaka and D. Inoue (Hakuto Co.), M. Nakata (Asahi Kogyosha Co.), Y. Shinozaki (Chuo Precision Co.), and

K. Yagi (Hewlett Packard Japan, Ltd.) for their cooperation in constructing the systems.

REFERENCES

[1] J. Kushibiki and N. Chubachi, "Acoustic microscopy for materials characterization," in *Proc. Ultrason. Int. 91 Conf.*, pp. 1–13, 1991.

[2] ——, "Material characterization by line-focus-beam acoustic microscope," *IEEE Trans. Sonics Ultrason.*, vol. SU-32, pp. 189–212, Mar. 1985.

[3] K. Yamanaka, J. Kushibiki, and N. Chubachi, "Anisotropy detection in hot-pressed silicon nitride by acoustic microscopy using the line-focus beam," *Electron. Lett.*, vol. 21, pp. 165–167, Feb. 1985.

[4] P. J. Burnett, G. A. D. Briggs, S. M. Al-Shukri, J. F. Duffy, and R. M. De La Rue, "Acoustic properties of proton-exchanged $LiNbO_3$ studied using the acoustic microscopy $V(z)$ technique," *J. Appl. Phys.*, vol. 60, pp. 2517–2522, Oct. 1986.

[5] J. Kushibiki, T. Ueda, and N. Chubachi, "Determination of elastic constants by LFB acoustic microscope," in *Proc. IEEE Ultrason. Symp.*, pp. 817–821, 1987.

[6] J. Kushibiki and N. Chubachi, "Application of LFB acoustic microscope to film thickness measurements," *Electron. Lett.*, vol. 23, pp. 652–654, Jun. 1987.

[7] C. K. Jen, C. Neron, J. F. Bussiere, L. Li, R. Lowe, and J. Kushibiki, "Characterization of cladded glass fibers using acoustic microscopy," *Appl. Phys. Lett.*, vol. 55, pp. 2485–2487, Dec. 1989.

[8] M. Obata, H. Shimada, and T. Mihara, "Stress dependence of leaky surface wave on PMMA by line-focus-beam acoustic microscope," *Exp. Mech.*, vol. 30, pp. 34–39, Mar. 1990.

[9] J. Kushibiki, T. Ishikawa, and N. Chubachi, "Cut-off characteristics of leaky Sezawa and pseudo-Sezawa wave modes for thin-film characterization," *Appl. Phys. Lett.*, vol. 57, pp. 1967–1969, Nov. 1990.

[10] J. Kushibiki, H. Takahashi, T. Kobayashi, and N. Chubachi, "Quantitative evaluation of elastic properties of $LiTaO_3$ crystals by line-focus-beam acoustic microscopy," *Appl. Phys. Lett.*, vol. 58, pp. 893–895, Mar. 1991.

[11] ——, "Characterization of $LiNbO_3$ crystals by line-focus-beam acoustic microscopy," *Appl. Phys. Lett.*, vol. 58, pp. 2622–2624, Jun. 1991.

[12] J. Kushibiki, T. Kobayashi, H. Ishiji, and N. Chubachi, "Elastic properties of 5-mol % MgO doped $LiNbO_3$ crystals measured by line focus beam acoustic microscopy," *Appl. Phys. Lett.*, vol. 61, pp. 2164–2166, Nov. 1992.

[13] C. K. Jen, Z. Wang, A. Nicolle, C. Neron, E. L. Adler, and J. Kushibiki, "Acoustic graded-index lenses," *Appl. Phys. Lett.*, vol. 59, pp. 1398–1400, Sep. 1991.

[14] T. Mihara and M. Obata, "Elastic constant measurement by using line-focus-beam acoustic microscope," *Exp. Mech.*, vol. 32, pp. 30–33, Mar. 1992.

[15] J. O. Kim, J. D. Achenbach, P. B. Mirkarimi, M. Shinn, and S. A. Barnett, "Elastic constants of single-crystal transition-metal nitride films measured by line-focus acoustic microscopy," *J. Appl. Phys.*, vol. 72, pp. 1805–1811, Sep. 1992.

[16] J. O. Kim, J. D. Achenbach, M. Shinn, and S. A. Barnett, "Effective elastic constants and acoustic properties of single-crystal TiN/NbN superlattices," *J. Mater. Res.*, vol. 7, pp. 2248–2256, Aug. 1992.

[17] C. K. Jen, C. Neron, A. Shang, K. Abe, L. Bonnell, and J. Kushibiki, "Acoustic characterization of silica glasses," *J. Amer. Ceram. Soc.*, vol. 76, pp. 712–716, Mar. 1993.

[18] Y. Ono, J. Kushibiki, and N. Chubachi, "Characterization of optical fiber preforms by line-focus-beam acoustic microscopy," in *Proc. IEEE Ultrason. Symp.*, pp. 1243–1246, 1993.

[19] J. Kushibiki, H. Ishiji, T. Kobayashi, and T. Sasamata, "Characterization of 36°YX $LiTaO_3$ wafers by line-focus-beam acoustic microscopy," *IEEE Trans. Ultrason., Ferroelect., Freq. Contr.*, vol. 42, pp. 83-90, Jan. 1995.

[20] Y. C. Lee, J. O. Kim, and J. D. Achenbach, "Acoustic microscopy measurement of elastic constants and mass density," *IEEE Trans. Ultrason., Ferroelect., Freq. Contr.*, vol. 42, pp. 253–264, Mar. 1995.

[21] A. Tourlog, J. D. Achenbach, and J. Kushibiki, "Line-focus acoustic microscopy measurements of acoustic properties of $LiTaO_3$ crystal plates with an inversion layer," *J. Appl. Phys.*, vol. 81, pp. 6616–6621, May 1997.

[22] J. Kushibiki, T. Kobayashi, H. Ishiji, and C. K. Jen, "Surface-acoustic-wave properties of MgO-doped $LiNbO_3$ single crystals measured by line-focus-beam acoustic microscopy," *J. Appl. Phys.*, vol. 85, pp. 7863–7868, Jun. 1999.

[23] T. Kobayashi, J. Kushibiki, and N. Chubachi, "Improvement of measurement accuracy of line-focus-beam acoustic microscope system," in *Proc. IEEE Ultrason. Symp.*, pp. 739–742, 1992.

[24] J. Kushibiki and M. Arakawa, "A method for calibrating the line-focus-beam acoustic microscopy system," *IEEE Trans. Ultrason., Ferroelect., Freq. Contr.*, vol. 45, pp. 421–430, Mar. 1998.

[25] W. Parmon and H. L. Bertoni, "Ray interpretation of the material signature in the acoustic microscope," *Electron. Lett.*, vol. 15, pp. 684–686, Oct. 1979.

[26] W. Kroebel and K.-H. Mahrt, "Recent results of absolute sound velocity measurements in pure water and sea water at atmospheric pressure," *Acustica*, vol. 35, pp. 154–164, Jun. 1976.

[27] J. M. M. Pinkerton, "The absorption of ultrasonic waves in liquids and its relation to molecular constitution," *Proc. Phys. Soc.*, vol. B20, pp. 129–141, Feb. 1949.

[28] J. Kushibiki, T. Sannomiya, and N. Chubachi, "A useful acoustic measurement system for pulse mode in VHF and UHF ranges," *IEEE Trans. Sonics Ultrason.*, vol. SU-29, pp. 338–342, Nov. 1982.

[29] J. Kushibiki and M. Arakawa, "Diffraction effects on bulk-wave ultrasonic velocity and attenuation measurements," *J. Acoust. Soc. Amer.*, vol. 108, pp. 564–573, Aug. 2000.

[30] J. Kushibiki, Y. Ono, and I. Takanaga, "Ultrasonic microspectroscopy of $LiNbO_3$ and $LiTaO_3$ single crystals for SAW devices," *Trans. IEICE C-I*, vol. J82-C-I, pp. 715–727, Dec. 1999.

[31] Y. Ono, J. Kushibiki, and N. Chubachi, "A measurement method of moving characteristics of precision mechanical-translation stages using ultrasonic plane waves and its application to a line-focus-beam acoustic microscopy system," *Trans. IEICE A*, vol. J78-A, pp. 279–286, Mar. 1995.

[32] J. Kushibiki, Y. Ohashi, and M. Arakawa, "Precise velocity measurements for thin specimens by line-focus-beam acoustic microscopy," *Jpn. J. Appl. Phys.*, vol. 38, pp. 89–91, Jan. 1999.

[33] ——, "Influence of reflected waves from the back surface of thin solid-plate specimen on velocity measurements by line-focus-beam acoustic microscopy," *IEEE Trans. Ultrason., Ferroelect., Freq. Contr.*, vol. 47, pp. 274–284, Jan. 2000.

[34] J. Kushibiki, T. Okuzawa, J. Hirohashi, and Y. Ohashi, "Line-focus-beam acoustic microscopy characterization of optical-grade $LiTaO_3$ single crystals," *J. Appl. Phys.*, vol. 87, pp. 4395–4403, May 2000.

[35] G. S. Kell, "Density, thermal expansivity, and compressibility of liquid water from 0° to 150°C: Correlations and tables for atmospheric pressure and saturation reviewed and expressed on 1968 temperature scale," *J. Chem. Eng. Data*, vol. 20, pp. 97–105, Jan. 1975.

[36] J. Kushibiki, I. Takanaga, M. Arakawa, and T. Sannomiya, "Accurate measurements of the acoustical physical constants of $LiNbO_3$ and $LiTaO_3$ single crystals," *IEEE Trans. Ultrason., Ferroelect., Freq. Contr.*, vol. 46, pp. 1315–1323, Sep. 1999.

[37] R. T. Smith and F. S. Welsh, "Temperature dependence of the elastic, piezoelectric, and dielectric constants of lithium tantalate and lithium niobate," *J. Appl. Phys.*, vol. 42, pp. 2219–2230, May 1971.

[38] J. J. Campbell and W. R. Jones, "Propagation of surface waves at the boundary between a piezoelectric crystal and a fluid medium," *IEEE Trans. Sonics Ultrason.*, vol. SU-17, pp. 71–76, Apr. 1970.

[39] H. J. McSkimin, "Measurement of elastic constants at low temperatures by means of ultrasonic waves—data for silicon and germanium single crystals, and for fused silica," *J. Appl. Phys.*, vol. 24, pp. 988–997, Aug. 1953.

[40] R. W. Keyes, "Device implications of the electronic effect in the elastic constants of silicon," *IEEE Trans. Sonics Ultrason.*, vol. SU-29, pp. 99–103, Mar. 1982.

[41] K. K. Liang, G. S. Kino, and B. T. Khuri-Yakub, "Material characterization by the inversion of $V(z)$," *IEEE Trans. Sonics Ultrason.*, vol. SU-32, pp. 213–224, Mar. 1985.

[42] Y. Sugawara, J. Kushibiki, and N. Chubachi, "Performance of concave transducers in acoustic microscopy," in *Proc. IEEE Ultrason. Symp.*, pp. 751–756, 1988.
[43] A. Kulik, G. Gremaud, and S. Sathish, "Direct measurements of the SAW velocity and attenuation using continuous wave reflection scanning acoustic microscope (SAMCRUW)," in *Accoustic Imaging*, H. Lee and G. Wade, Eds. New York: Plenum, 1991, pp. 227–235.
[44] Y. Ono and J. Kushibiki, "Experimental study of construction mechanism of V(z) curves obtained by line-focus-beam acoustic microscopy," *IEEE Trans. Ultrason., Ferroelect., Freq. Contr.*, vol. 47, pp. 1042–1050, Jul. 2000.
[45] J. Kushibiki, T. C. Wei, Y. Ohashi, and A. Tada, "Ultrasonic microspectroscopy characterization of silica glass," *J. Appl. Phys.*, vol. 87, pp. 3113–3121, Mar. 2000.
[46] J. Kushibiki, Y. Ohashi, and Y. Ono, "Evaluation and selection of $LiNbO_3$ and $LiTaO_3$ substrates for SAW devices by the LFB ultrasonic material characterization system," *IEEE Trans. Ultrason., Ferroelect., Freq. Contr.*, vol. 47, pp. 1068–1076, Jul. 2000.
[47] J. Kushibiki, M. Miyashita, and N. Chubachi, "Quantitative characterization of proton-exchanged layers in $LiTaO_3$ optoelectronic devices by line-focus-beam acoustic microscopy," *IEEE Photonics Technol. Lett.*, vol. 8, pp. 1516–1518, Nov. 1996.
[48] J. Kushibiki and M. Miyashita, "Characterization of domain-inverted layers in $LiTaO_3$ by line-focus-beam acoustic microscopy," *Jpn. J. Appl. Phys.*, vol. 36, pp. 959–961, Jul. 1997.
[49] ——, "Quantitative evaluation of fabrication processes of proton-exchanged layers in $LiTaO_3$ optoelectronic devices by the line-focus-beam ultrasonic material characterization system," *J. Appl. Phys.*, vol. 89, pp. 2017–2024, Feb. 2001.
[50] J. Kushibiki and I. Takanaga, "Elastic properties of single- and multi-domain crystals of $LiTaO_3$," *J. Appl. Phys.*, vol. 81, pp. 6906–6910, May 1997.
[51] I. Takanaga and J. Kushibiki, "Elastic constants of multi-domain $LiTaO_3$ crystal," *J. Appl. Phys.*, vol. 86, pp. 3342–3346, Sep. 1999.
[52] J. Kushibiki, I. Takanaga, and S. Nishiyama, "Accurate measurements of the acoustical physical constants of synthetic α-quartz for SAW devices," *IEEE Ultrason., Ferroelect., Freq. Contr.*, vol. 49, no. 1, pp. 125–135, 2002.

Jun-ichi Kushibiki (M'83) was born in Hirosaki, Japan on November 23, 1947. He received the B.S., M.S., and Ph.D. degrees in electrical engineering from Tohoku University, Sendai, Japan in 1971, 1973, and 1976, respectively.

In 1976, he became a research associate at the Research Institute of Electrical Communication, Tohoku University. In 1979, he joined the Department of Electrical Engineering, Faculty of Engineering, Tohoku University, where he was an associate professor from 1988 to 1993 and became a professor in 1994. He has been studying ultrasonic metrology, especially acoustic microscopy and its applications, and has established a method of material characterization by line-focus-beam acoustic microscopy. He also has been interested in biological tissue characterization in the higher frequency range, applying both bulk and acoustic microscopy techniques.

Dr. Kushibiki is a fellow of the Acoustical Society of America, and member of the Institute of Electronics, Information and Communication Engineers of Japan; the Institute of Electrical Engineers of Japan; the Acoustical Society of Japan; and the Japan Society of Ultrasonics in Medicine.

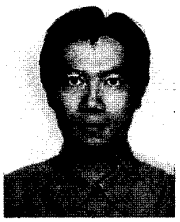

Yuu Ono (M'99) was born in Yamanashi Prefecture, Japan on March 18, 1967. He received the B.S., M.S., and Ph.D. degrees in electrical engineering from Tohoku University, Sendai, Japan in 1990, 1992, and 1995, respectively.

In 1995, he became a research associate at the Department of Electrical Engineering, Faculty of Engineering, Tohoku University, where he worked on the development of the line-focus-beam acoustic microscopy system and its application to material characterization. In 2001, he was offered a visiting fellowship in Canadian Government Laboratories and joined the Industrial Materials Institute, National Research Council of Canada. His research interests include material characterization and material process monitoring using ultrasound.

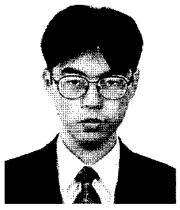

Yuji Ohashi was born in Toyama prefecture, Japan on August 27, 1973. He received the B.S. and M.S. degrees in electrical engineering from Tohoku University, Sendai, Japan in 1996 and 1999, respectively.

He is currently studying toward the Ph.D. degree at Tohoku University. His research interests include development of line-focus-beam acoustic microscopy system and its application to materials characterization.

Mr. Ohashi in a member of the Acoustical Society of Japan.

Mototaka Arakawa (M'00) was born in Sendai, Japan on January 19, 1971. He received the B.S., M.S., and Ph.D. degrees in electrical engineering from Tohoku University, Sendai, Japan in 1993, 1995, and 2000, respectively.

In 2000, he became COE Research Fellow at the Research Institute of Electrical Communication, Tohoku University. In 2001, he became a research associate at the Department of Electrical Engineering, Faculty of Engineering, Tohoku University. His research interests include developments of the measurement methods of elastic constants of solid materials and of the calibration method of the line-focus-beam acoustic microscopy system.

Dr. Arakawa is a member of the Acoustical Society of Japan and the Institute of Electronics, Information, and Communication Engineers of Japan.